15

Oxide-Matrix Based Nanocomposite Materials for Advanced Magnetic and Optical Functionalities

Eva Pellicer[1], Emma Rossinyol[1,2], Moisés Cabo[1], Alberto López-Ortega[3], Marta Estrader[3], Santiago Suriñach[1], Maria Dolors Baró[1], Josep Nogués[4] and Jordi Sort[5]
[1]*Departament de Física, Facultat de Ciències, Universitat Autònoma de Barcelona,*
[2]*Servei de Microscòpia, Universitat Autònoma de Barcelona,*
[3]*Centre d'Investigació en Nanociència i Nanotecnologia (ICN-CSIC), Campus Universitat Autònoma de Barcelona,*
[4]*Institució Catalana de Recerca i Estudis Avançats (ICREA) and Centre d'Investigació en Nanociència i Nanotecnologia (ICN-CSIC), Campus Universitat Autònoma de Barcelona,*
[5]*Institució Catalana de Recerca i Estudis Avançats (ICREA) and Departament de Física, Universitat Autònoma de Barcelona,*
E-08193 Bellaterra,
Spain

1. Introduction

Advanced engineering applications often require multifunctional materials with a wide range of tunable properties. Such a technological demand is usually difficult to fulfill using single-phase materials. Hence, there is an increasing need to combine materials with dissimilar properties, in a synergetic manner, to achieve certain technological goals. This has prompted the development of novel types of composite materials and the concomitant implementation of innovative processing routes. Examples of currently used composite materials are: polymer-matrix composites, metal-matrix composites or ceramic-metal mixtures (also termed *cermets*), among others (Ajayan et al., 2003).

Some of the properties of composite materials (e.g., mechanical hardness, fracture toughness or coercivity) are often enhanced when their crystalline structure is refined towards the nanoscale. Similarly, physical and chemical properties related to interfacial effects (e.g., magnetic exchange bias or catalytic efficiency), are also improved in nanocomposite structures with respect to coarse-grained multi-component materials. Furthermore, some interesting size effects (e.g., quantum effects) can also emerge in materials whose structure is made nanocrystalline. These novel effects have triggered the interest for *nanocomposite materials*, where at least one of their counterparts shows crystallite sizes typically below 100 nm. Although many of the technological applications of nanocomposite materials benefit from their outstanding mechanical properties, in this work we focus our attention on other types of properties (magnetic and optical) exhibited by a particular type of composite

materials made of an oxide matrix in which either a metal, another oxide or a semiconductor are embedded or in intimate contact. More specifically, we have investigated the properties of nanocomposite materials consisting of: (i) hard ferromagnetic (FM) $SmCo_5$ particles exchange coupled to an antiferromagnetic (AFM) NiO matrix, prepared by mechanical milling; (ii) mesoporous $NiO/NiCo_2O_4/Co_3O_4$ composite materials prepared using a multi-step nanocasting approach and (iii) CdS-filled mesoporous SiO_2 matrices also prepared by a nanocasting strategy. While systems (i) and (ii) are appealing from a magnetic viewpoint, system (iii) shows interesting and novel optical properties.

2. Enhanced magnetic properties in hard ferromagnetic particles embedded in an oxide matrix

The large variety of ferromagnetic materials that exist in nature can be roughly classified into two categories: soft and hard ferromagnetic materials. Soft ferromagnetic materials are characterized by low values of coercivity, H_C, typically lower than 10 Oe, and large values of saturation magnetization, M_S, usually higher than 100 emu/g. This results in narrow hysteresis loops [see Figure 1(a)]. Some examples of soft FM materials are Fe, Ni, permalloy or FeSi alloys. They are used in, for example, electromagnets or transformers cores. On the contrary, hard FM materials, which are also known as *permanent magnets*, are characterized by high values of H_C, typically larger than 500 Oe, and usually smaller values of M_S than soft magnetic materials, i.e. wide hysteresis loops [see Figure 1 (b)]. Some examples of hard FM are $SmCo_5$, Al-Ni-Co alloys or $Nd_2Fe_{14}B$. Permanent magnets have lots of applications in industry: in motors and generators, telecommunications (headphones, magnetic sensors, high-density magnetic recording media, …), in synchrotrons (as systems for particles guidance), etc. (Hadjipanayis, 1999).

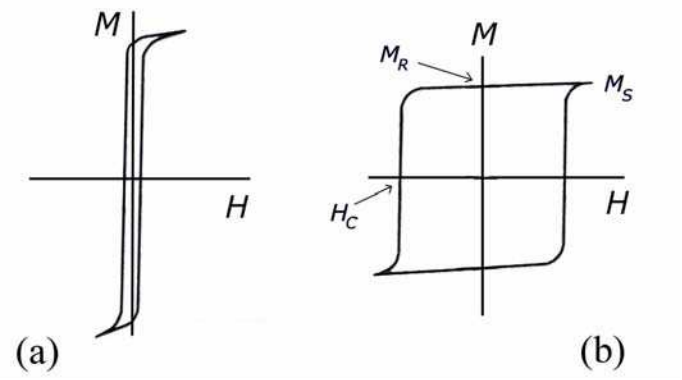

Fig. 1. Hysteresis loops of (a) a soft magnetic material and (b) a hard magnetic material.

The figure of merit of a hard magnetic material is its *energy product*, which is denoted by $(BH)_{Max}$, and is roughly proportional to the total area enclosed by the hysteresis loop. The values of $(BH)_{Max}$ give a good estimation of the quality of the hard magnetic material, since it is closely related to the overall energy that can be stored in the magnet. Obviously, magnets with higher $(BH)_{Max}$, would require smaller sizes to have the same efficiency. In order to maximize $(BH)_{Max}$ it is necessary to have a large H_C, high values of M_S and a squareness ratio, M_R/M_S (where M_R is the remanent magnetization), as close to 1 as possible. The result of increasing H_C

is a widening of the hysteresis loop, while increasing M_S results in a lengthening of the loop along the magnetization axis. Finally, an increase of M_R/M_S makes the loop squarer. The net effect in all three cases is an enhancement of the energy product. Figure 2 shows a historical evolution of the maximum energy product, $(BH)_{Max}$, that has been accomplished during the last century in different types of hard FM materials.

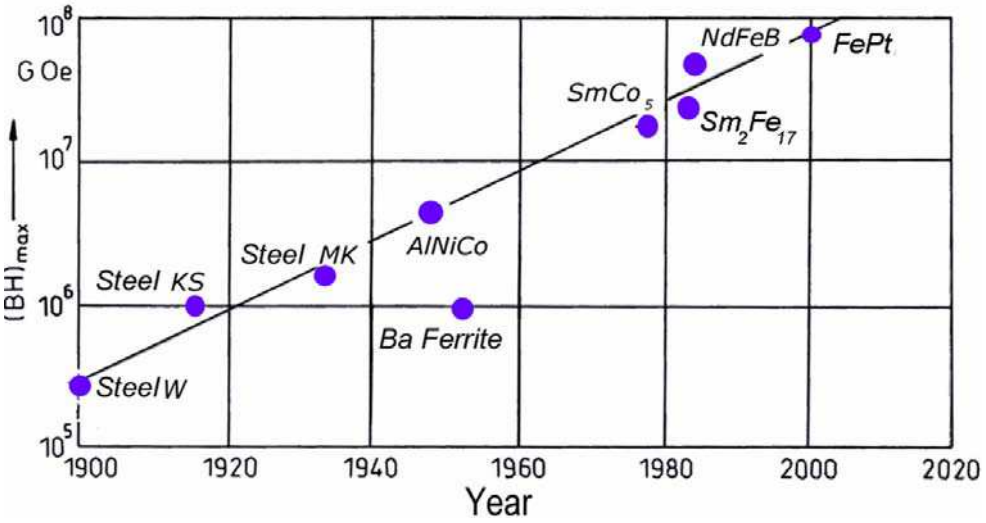

Fig. 2. Chronological evolution of the energy product values, at room temperature, in permanent magnetic materials during the last decades.

Permanent magnet development has been traditionally based on the search for materials with a large magnetocrystalline anisotropy and/or reduction of the particle size to obtain isolated single-domain particles (Hadjipanayis, 1999). In recent years, processing of hard and soft magnetic composites (termed spring magnets) has also been used to improve permanent magnet properties. Exchange interactions between hard and soft grains bring about an increase of the saturation magnetization (M_S) of the composites. This increase of M_S, despite of the reduction of the coercivity (H_C), produces an increase of their energy product, $(BH)_{Max}$, of the magnet (Kneller & Hawig, 1991). In this work, we demonstrate that similar to what is observed in thin film systems (Nogués & Shculler, 1999), inducing an exchange interaction between FM and AFM powder materials results in an enhancement of both H_C and the M_R/M_S ratio of the hard magnet.

In our case, the coupling is accomplished by a mechanical grinding process of the FM ($SmCo_5$) and AFM (NiO) components. As in spring magnets, under suitable conditions an increase of the $(BH)_{Max}$ of the FM can also be achieved (Sort et al., 2002). A typical scanning electron microscopy image, corresponding to $SmCo_5$ particles embedded in a NiO matrix (in a weight ratio 1:1) is shown in Figure 3.

Typically, a cooling treatment under a magnetic field from above the Néel temperature of the AFM phase is required in order to induce FM-AFM exchange interactions. In our case, no heating/cooling was purposely performed on the as-milled powders. However, it is well-known that, due to the impacts between the powder and balls, temperature can locally rise significantly during the milling, eventually exceeding the Néel (or blocking)

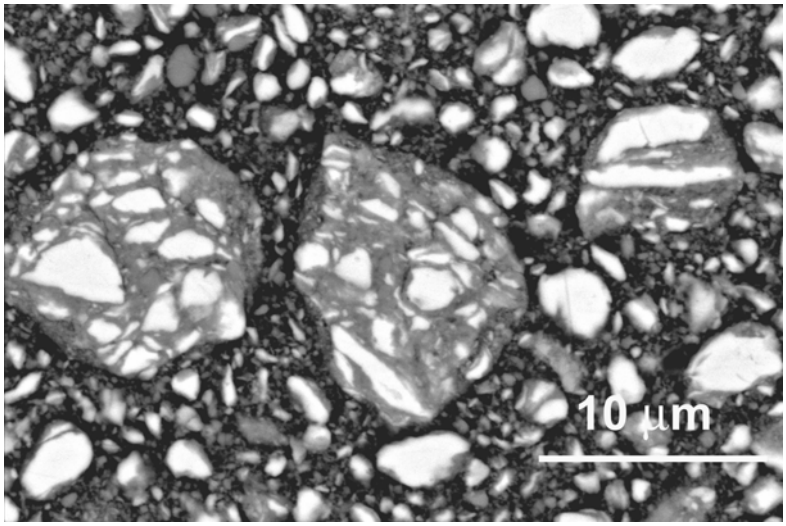

Fig. 3. Scanning electron microscopy image of $SmCo_5$ particles (light) embedded in a NiO matrix (grey). The image corresponds to $SmCo_5$ milled with NiO, for 32 h, in a weight ratio 1:1.

temperature of the system (Murty & Ranganathan, 1998). As a result, and due to the stray fields emanated from $SmCo_5$ grains, an exchange interaction is likely to be set during the milling of this composite material due to an instantaneous heating/cooling process caused by the above mentioned impacts. Consequently, the spins of the AFM grains located near the interfaces with the FM particles will tend to align towards the directions of the neighbouring FM domains (see Figure 4). During magnetic field switching, the FM-AFM coupled grains will tend to reverse together but since they are exchange-coupled the coercivity will increase.

As milling proceeds, the crystallite sizes of the different phases which form the composite material (i.e., $SmCo_5$ and NiO) progressively decrease. The obtained values of coercivity are particularly large for intermediate $SmCo_5$ crystallite sizes and larger AFM weight fractions (see Figure 5).

Actually, several factors have to be taken into account in order to explain the milling time dependence of H_C in ball milled $SmCo_5$ and $SmCo_5$ + NiO powders. As shown in Figure 5, H_C increases for short milling times in $SmCo_5$ either when it is milled alone or with NiO. This can be mainly attributed to the particle size reduction associated with the milling process. Indeed, the unmilled $SmCo_5$ particles are several μm in size. Therefore, they are mainly in a multidomain state. However, as the milling time increases, the FM particles fracture and become smaller. Thus, many of them reach sizes of around 1 μm (see Figure 3). Therefore, after intermediate milling times, a fraction of $SmCo_5$ particles may be in a monodomain state. This can be the reason for the increase of H_C during the first stages of the mechanical milling process, although small defects acting as pinning sites could also play some role. However, for long enough milling times H_C is found to significantly reduce. We have attributed this reduction to the high degree of structural disorder generated in $SmCo_5$ after long-term milling, which results in a decrease of its magnetic anisotropy and, thus, of its coercivity (Strnat & Strnat, 1991; Leslie-Pelecky & Schalek, 1999).

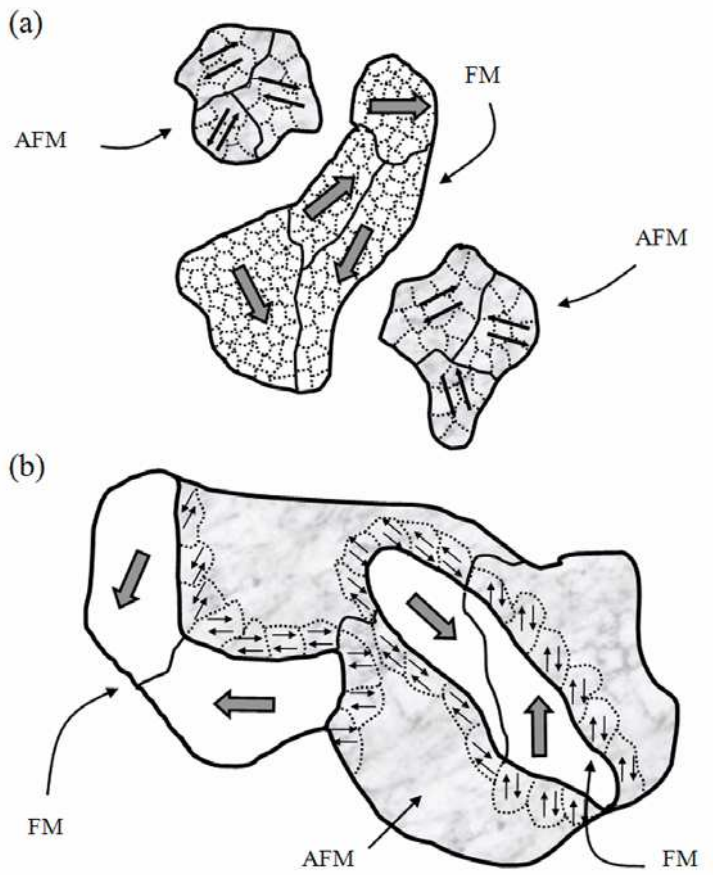

Fig. 4. Intuitive illustration of the morphology and spin configuration of $SmCo_5$ + NiO powders ball milled together. In (a) the morphology after short-term milling is illustrated, i.e. the FM and AFM particles are still not soldered together. In particular, one FM and two AFM particles are represented, each of them containing a few magnetic domains, which, at the same time, include several crystallites. Note that in (a) the spins in the FM and the AFM do not interact with each other and, consequently, the magnetization directions in the different domains are at random. Panel (b) represents the morphology generated after long-term milling. In this case, two FM particles have soldered with AFM powders to form one FM-AFM agglomerate. For simplicity, only the crystallites in the AFM located at the interfaces with the FM particles have been represented. The figure shows that, if one assumes that some FM-AFM exchange interactions are induced during the milling, the spins of the AFM grains located near the interfaces with the FM particles will tend to align towards the directions of the neighboring FM domains. This coupling at the interface will result in the local exchange bias effects, i.e. an enhancement of coercivity.

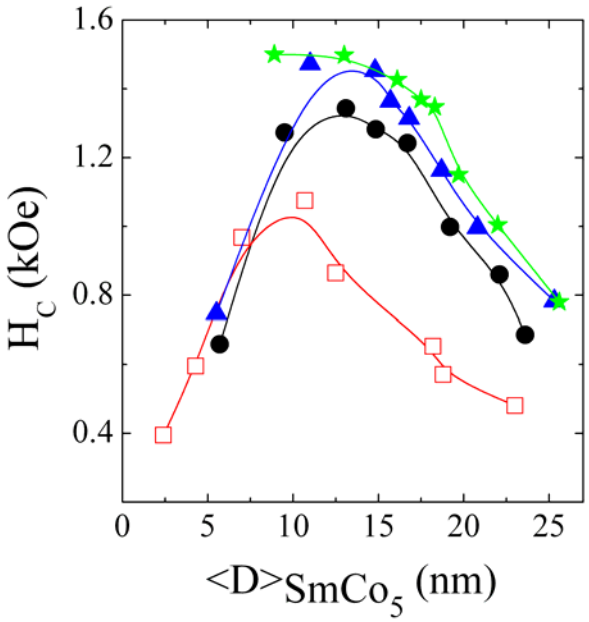

Fig. 5. Dependence of the coercivity, H_C, on the $SmCo_5$ crystallite size (which is, in turn, tuned by varying the milling time) for $SmCo_5$:NiO milled in a weight ratio of 1:0 (-□-), 3:1 (-●-), 3:2 (-▲-) and 1:1 (-★-). The lines are a guide to the eye.

The increase of H_C with the NiO content is due to an enhancement of FM-AFM exchange interactions. In order to verify the role of NiO in this H_C increase, ball milling of $SmCo_5$ was also performed with CoO (which is paramagnetic at room temperature). As shown in Figure 6, the structural refinement of $SmCo_5$ crystallite size during ball milling is similar than for NiO (values as small as 10 nm are obtained after long-term milling, e.g. 32 h). It can be seen that, in the three cases, the maximum H_C is obtained for $\langle D \rangle_{SmCo5}$ of the order of 10-15 nm. Moreover, Figure 6 also shows that for a fixed crystallite size, H_C remains higher in $SmCo_5$ + CoO than for $SmCo_5$ milled alone. This behavior can be understood in terms of the role that the paramagnetic CoO matrix plays in isolating the different $SmCo_5$ grains. This isolation brings about a decrease of the interparticle FM-FM exchange interactions, which are known to reduce H_C due to the cooperative reversal of several interacting FM particles (Schrefl et al., 1994). Nevertheless, the fact that, for a fixed $SmCo_5$ crystallite size, H_C is even higher when it is milled with NiO can be taken as a confirmation that FM-AFM exchange interactions are actually present in the as-milled $SmCo_5$ + NiO powders.

In spite of the coercivity enhancement, the presence of NiO inevitably results in a reduction of the overall saturation magnetization of the composite (due to the zero net magnetization of the AFM phase), which is again proportional to the NiO content. Hence, $(BH)_{Max}$ is reduced when the NiO content is increasingly high, as for example in the case of the 1:1 ratio (see Figure 7). Nevertheless, due to the coercivity increase associated with the FM-AFM coupling, $(BH)_{Max}$ in 3:1 $SmCo_5$:NiO (with $SmCo_5$ crystallite size around 15 nm, corresponding to a milling time of 4 h) is enhanced with respect to $SmCo_5$ alone.

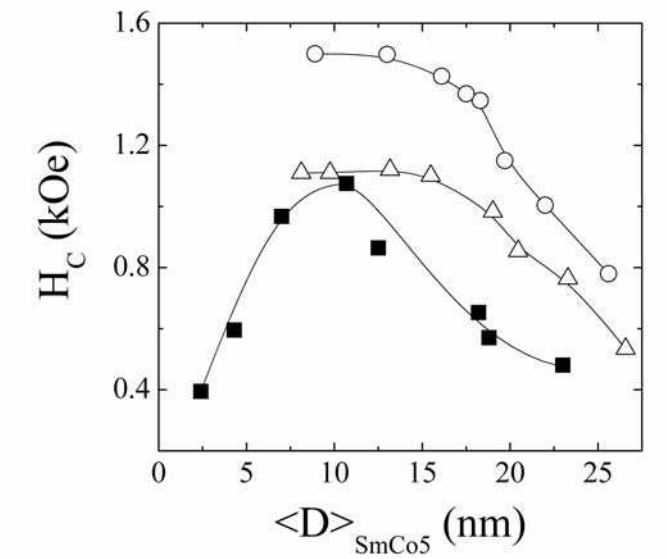

Fig. 6. Dependence of the coercivity, H_C, on $SmCo_5$ crystallite size, $\langle D \rangle_{SmCo5}$, for $SmCo_5$ milled alone (—■—), with CoO (—Δ—) and NiO (—O—) in the weight ratio 1:1. The lines are a guide to the eye.

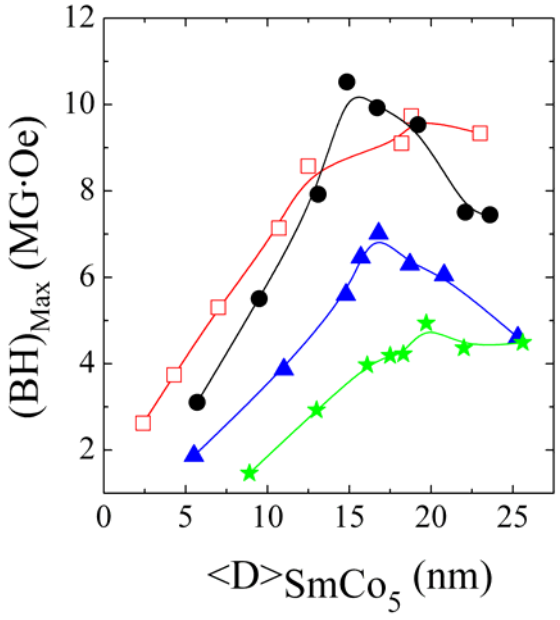

Fig. 7. Dependence of the energy product, $(BH)_{Max}$, on the $SmCo_5$ crystallite size (which is, in turn, tuned by varying the milling time) for $SmCo_5$:NiO milled in a weight ratio of 1:0 (-□-), 3:1 (-●-), 3:2 (-▲-) and 1:1 (-★-). The lines are a guide to the eye.

It is noteworthy that, due to the interplay of all the different effects, the enhancement of $(BH)_{Max}$ in this class of materials needs optimization of both the milling time and the FM:AFM weight ratio. Figure 8 summarizes the maximum values of H_C and $(BH)_{Max}$ that can be achieved in $SmCo_5$-NiO composite materials after proper optimization of the milling time and FM:AFM weight percentage.

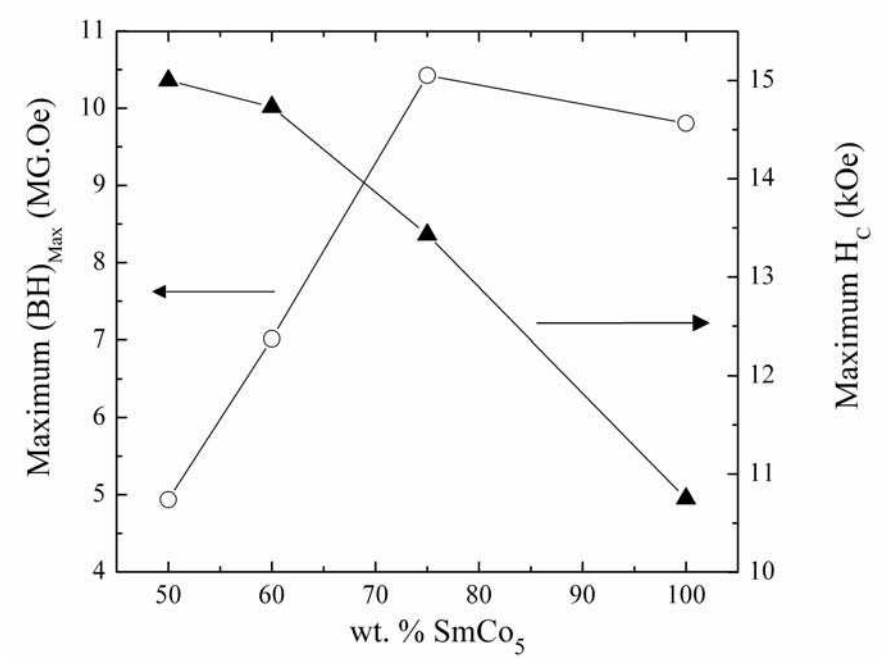

Fig. 8. Dependence of the maximum achievable values of coercivity, H_C, and energy product, $(BH)_{Max}$, as a function of the $SmCo_5$ weight percentage. The values plotted correspond to the milling times that give maximum H_C and $(BH)_{Max}$ for each composition.

3. Tunable magnetic behaviour in oxide-oxide composite materials synthesized by nanocasting approach

Unlike ball-milling, which is a quite unique top-down approach for the synthesis of nanostructured composite materials, other approaches such as the template-assisted methods based on a bottom-up strategy are also currently receiving a great deal of attention. Among them, the multi-step nanocasting method is based on the confined growth of transition metal oxides, metals and metal chalcogenides within the pores of ordered inorganic matrices (Lu et al., 2010). Mesoporous silicas, which are characterized by ordered arrays of porous with diameters in the range between 2 nm and 50 nm, are the key materials in the field of 'host-guest chemistry'.

Since the first mesoporous silica material, MCM-41, was discovered by scientists of the Mobil Corporation in 1992 (Beck et al., 1992), several mesoporous silica structures have been developed (e.g. SBA-15, KIT-6, SBA-16, FDU-1, to name a few). The main difference between these silica structures relies on pore topology. While SBA-15 and KIT-6 feature channel-type

mesopores accessible from outside, SBA-16 and FDU-1 consist of much less accessible cage-like cavities interconnected by narrow throats. Typically, the silica hosts, which are themselves prepared by templating procedures, are impregnated with suitable precursors. When the confined growth of a transition metal oxide is pursued, the precursor is usually a nitrate salt. Among the impregnation procedures available, the so-called evaporation, solid-liquid and two-solvent methods are the most employed so far. The precursor:silica molar ratio as well as the number of impregnation steps must be carefully controlled in order to maximize the filling of the silica host while avoiding the growth of non-mesoporous particles outside the mesoporous silica structure. The impregnated silicas are then calcined in atmospheric conditions to convert the nitrate salt into the corresponding oxide, thereby yielding a $SiO_2@Me_xO_y$ (Me = metal) nanocomposite (Figure 9). Further etching of the SiO_2 matrix can be done with diluted NaOH or HF solutions to obtain the Me_xO_y as negative replica of the SiO_2 host.

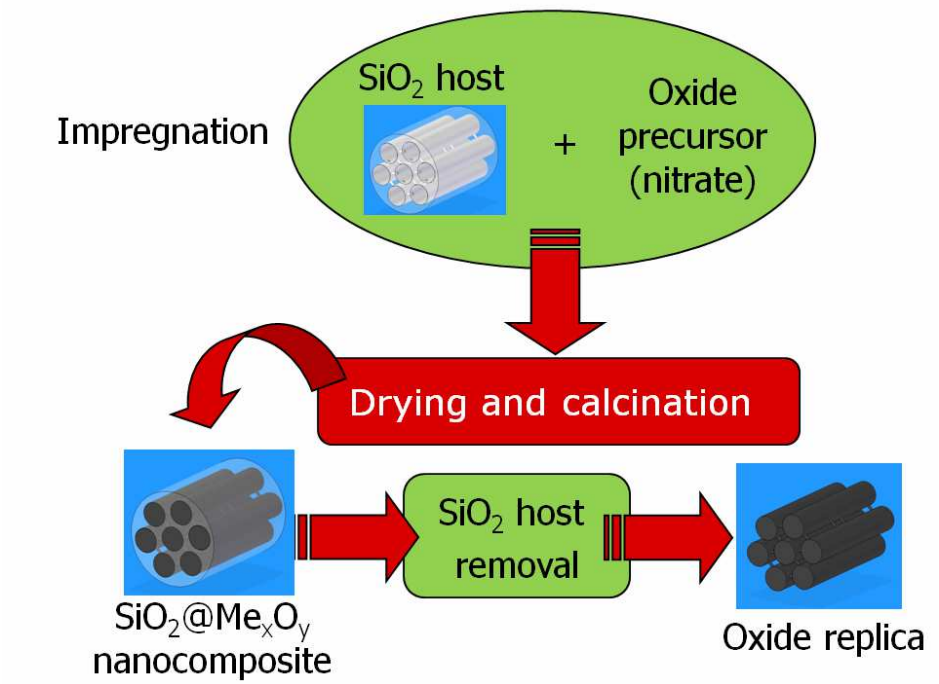

Fig. 9. Sketch of nanocasting pathway for the synthesis of $SiO_2@Me_xO_y$ nanocomposites. Further selective etching of the SiO_2 matrix releases the Me_xO_y as a negative replica of the SiO_2 host.

Figure 10 shows transmission electron microscopy (TEM) images of SBA-15 SiO_2 and of $SiO_2@Co_3O_4$ composite synthesized using the former as a host. The SBA-15 silica consists of a well-ordered hexagonal array of one-dimensional channels, whose diameter can be typically varied in the range of 6–15 nm depending on the synthesis conditions. Here, impregnation of the silica host (pore size around 7 nm) with the metal oxide precursor was carried out by evaporation: the silica powder was suspended in ethanol and put in contact

with a given amount of cobalt nitrate salt, stirred for 24 h and left for ethanol evaporation. Then, a calcination at 550ºC made it possible to convert the precursor into AFM Co_3O_4, whose growth took place inside the silica channels. The darker areas in the TEM image correspond to the Co_3O_4 material confined within the silica mesopores. A similar procedure was carried out taking AFM NiO and ferrimagnetic (FiM) $NiCo_2O_4$ spinel as guest materials. It is noteworthy that these oxides are highly crystalline. This is related to the excellent thermal stability of the silica skeleton, which allows a relatively high calcination temperature. In contrast, for sol-gel or soft-templating approaches, the heating temperatures are much more restrictive.

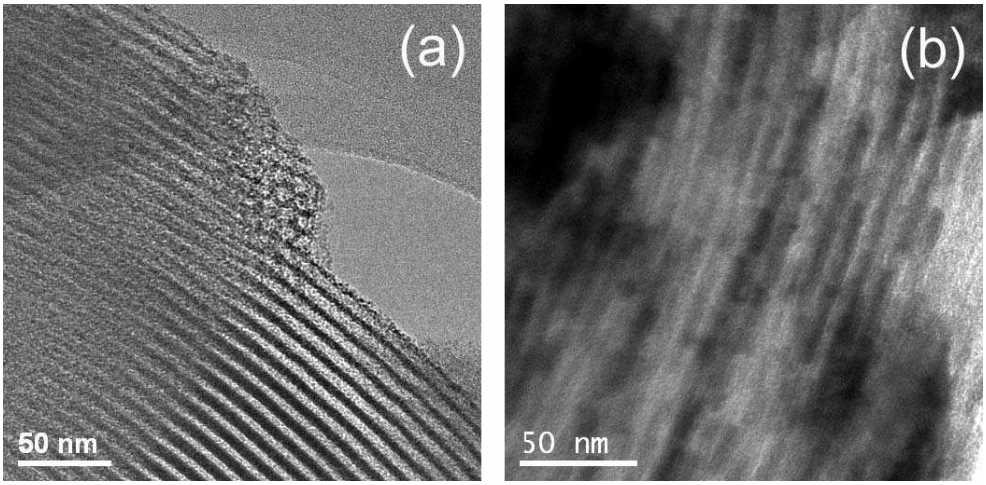

Fig. 10. TEM images of (a) SBA-15 SiO_2 template and (b) Co_3O_4-filled SBA-15 SiO_2.

As mentioned before, release of the guest material confined within the silica channels is feasible using diluted NaOH or HF solutions to selectively etch the silica host, leading to transition metal oxides displaying ordered arrangements of mesopores with high surface areas. To date, most of the works concerning the synthesis of mesorelief metal oxides rely on single metal oxides (e.g WO_3, In_2O_3, CeO_2, Co_3O_4, NiO, Fe_3O_4) (Tiemann, 2008). Application of these materials in many different fields like heterogeneous catalysis, gas-sensing, optics, etc. has been already demonstrated but there is still room to explore new functionalities, in particular from the magnetic perspective. In this sense, we have tackled the synthesis of compositionally graded oxide-oxide composites, namely $NiO/NiCo_2O_4/Co_3O_4$, *via* replication of SBA-15 silica template. For this purpose, the SBA-15 silica host was impregnated with nickel and cobalt nitrate salts in different Ni(II):Co(II) molar ratios following the evaporation method above described. The impregnated silica was then calcined at 550ºC and the SiO_2 template further removed. Selective etching of the SiO_2 host was carried out in diluted NaOH solution under stirring for 24 h. The $NiO/NiCo_2O_4/Co_3O_4$ nanocomposite powders were collected after centrifugation and decanted off the supernatant, thoroughly rinsed in ethanol and finally dried in vacuum. Depending on the nominal Ni(II):Co(II) molar ratio, either NiO-rich or $NiCo_2O_4$-rich nanocomposites can be obtained. From the morphology viewpoint, hexagonally-arranged cylindrical nanowires were obtained for high Co(II):Ni(II) molar ratios, whilst randomly organized rods were obtained for low Co(II):Ni(II) ratios. The diameter of these

nanorods/nanowires is around 8 nm (or slightly less), which correlates nicely with the pore size of the parent SBA-15 silica owing to the confined growth of the solid within the silica channels. Also, the composites are highly crystalline as demonstrated by high-resolution TEM images and X-ray diffraction patterns (not shown).

The distinct magnetic character of the constituent phases ($NiCo_2O_4$ is FiM while NiO and Co_3O_4 are AFM) allows to properly tune the magnetic behaviour of the final composite (Cabo et al., 2010). Figure 11 shows the dependence of the saturation magnetization, M_S, of these hybrid materials as a function of the $NiCo_2O_4$ amount. The M_S values were extracted from the corresponding hysteresis loops at 10K after substracting the linear contribution. It is noteworthy that the magnetization did not saturate at the maximum applied field of 70 kOe due to the presence of the AFM phases (NiO and Co_3O_4) and magnetic disorder effects usually observed at the nanoscale (Batlle & Labarta, 2002). Although M_S depends linearly on the amount of $NiCo_2O_4$, the coercivity varies non-monotonically, giving rise to values between 170 Oe and 1600 Oe, caused mainly by the AFM-FiM coupling (Nogués & Schuller, 1999) of the composites.

Significantly, the rich-$NiCo_2O_4$ composites are still FiM at room temperature, which means that the superparamagnetic blocking temperature, T_B, is above 300 K. Such enhanced T_B may arise from an increase of the effective anisotropy due to the shape anisotropy and the FiM-AFM exchange coupling. This makes it possible to foresee innovative applications for these nanocomposites since the powders could be trapped or guided to specific locations by using small magnetic fields. Such attribute could be exploited, for instance, in magnetic hyperthermia applications.

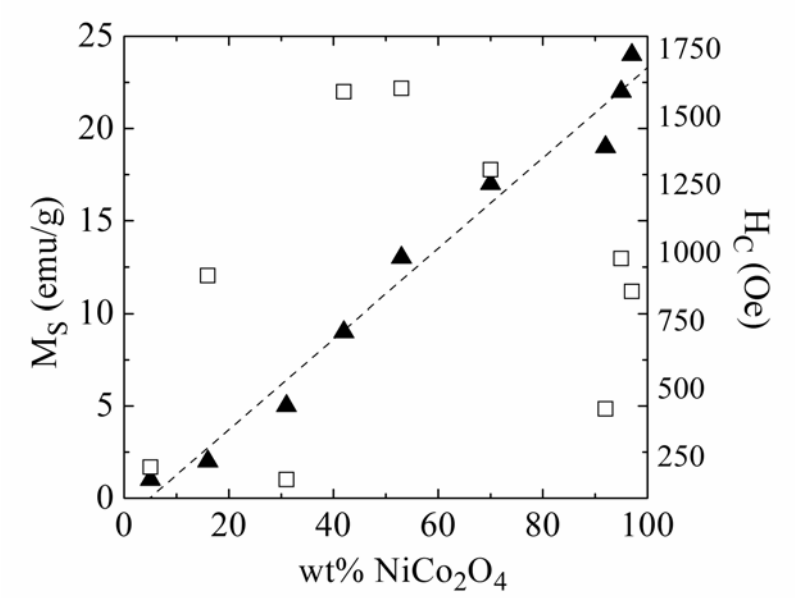

Fig. 11. Saturation magnetization (▲) and coercivity (□) (at T = 10 K) dependence of the nanocomposites with the amount of FiM $NiCo_2O_4$. The amount of $NiCo_2O_4$ was estimated by Rietveld refinement of the corresponding X-ray diffraction patterns. The dashed line is an eye-guide.

Although the replication process entailed the loss of some mesostructural order, the Brunauer-Emmett-Teller (BET) area of the composites is in the range of 60-80 m^2/g, which can be considered as moderately large. Hence, these materials benefit from reasonably high surface areas and tunable magnetic properties. Remarkably, other silica mesostructures can be used to obtain mesorelief oxide-oxide nanocomposites. As an example, we show a TEM image of a $NiCo_2O_4$-NiO nanocomposite obtained using SiO_2 KIT-6 as a template [Fig. 12(a)] together with its corresponding magnetic hyteresis loop [Fig. 12(b)]. Unlike the SBA-15 silica, the KIT-6 one displays a gyroidal structure characterized by a 3D interpenetrating network of channels. The corresponding replicas typically feature hexagonal rings like the one shown in Figure 12(a).

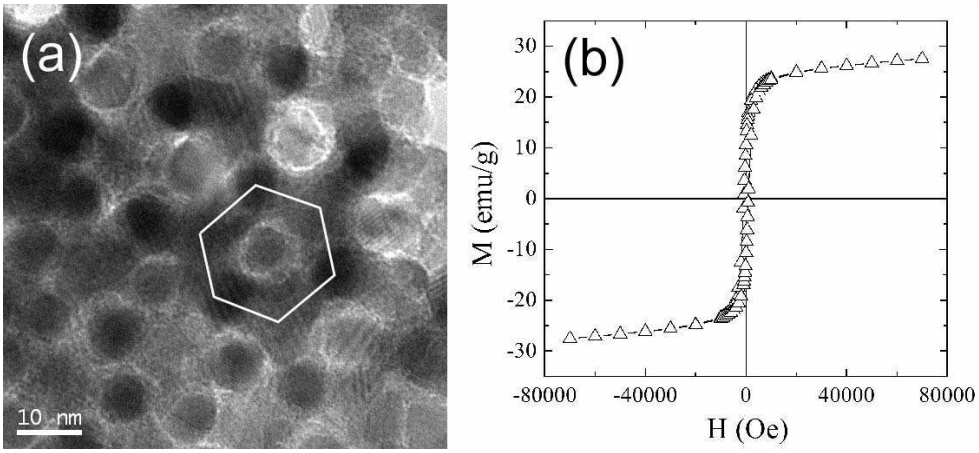

Fig. 12. (a) TEM image of a KIT-6 templated $NiCo_2O_4$-NiO (7 wt% NiO) composite (notice the hexagonal rings typical of this mesostructure) and (b) its corresponding hysteresis loop at 10 K.

4. Novel optical properties in semiconductor materials confined in mesoporous silica matrices

If the confined material within the silica channels is not a metal oxide but a metal chalcogenide, that is, a II−VI semiconductor like CdSe, CdTe or CdS, then the optical properties of the resulting composite can be exploited (Li et al., 2008). The synthesis of II−VI semiconductor nanocrystals has been extensively investigated both from fundamental and applied standpoints due to their luminosity, nonlinear optical properties and quantum effects, making them excellent for applications in electrical, photoelectrical and biologic devices. Compared to the case of transition metal oxides, the confined growth of metal chalcogenides within silica templates has been much less explored, mainly because of the need of non-commercial, hybrid precursors able to render the metal calchogenide at temperatures well below the formation of cadmium oxide. For this reason, instead of using a single-source precursor, other strategies like the Cd^{2+} ion exchange reaction in the inner pores of mesoporous silica during a treatment with H_2S gas have also been attempted (Wang et al., 2002).

Here we show that the photoluminescence properties of CdS nanocrystals embedded in silica matrices and derived from a single-source precursor differ from the behavior displayed by the mesorelief nanocrystals. Different silica mesostructures (i.e. SBA-16, KIT-6 and SBA-16) were impregnated with cadmium thioglycolate. The heat-treatment was carried out at low temperature in two stages (120 and 160ºC) to render CdS. A TEM image of the SBA-15 SiO_2@CdS composite is shown in Figure 13(a), in which the location of the CdS can be identified by the darker regions. Figure 13(b) shows a HRTEM image of the highly-crystalline CdS replica obtained following template removal. The CdS replica is composed of nanocrystals arranged in the form of wires (an image at lower magnification is shown in the inset, where the SBA-15 mesostructure can be clearly identified).

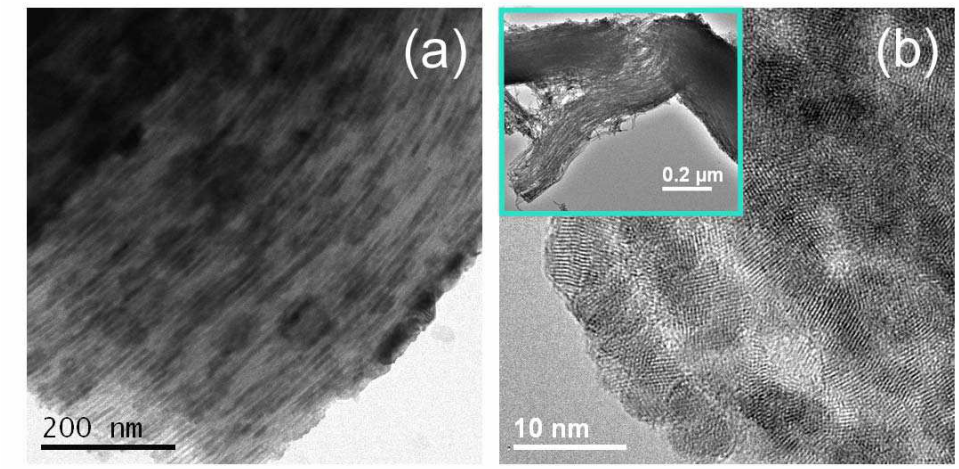

Fig. 13. TEM image of (a) SBA-15 SiO_2@CdS composite and (b) *free* CdS nanocrystals in SBA-15 structure (a view at lower magnification is shown in the inset).

A comparison of the normalized photoluminescence (PL) spectra acquired at room temperature using a confocal laser scanning microscope (CLSM) in the 435 – 774 nm range for both samples is presented in Figure 14(a). The samples were excited at 405 nm (near-UV) laser wavelength. Compared to pure CdS replica, the emission band of the SBA-15 SiO_2@CdS composite broadens and its maximum is shifted to shorter wavelengths. Similar results were observed for KIT-6 SiO_2@CdS composite when compared with its corresponsing CdS replica [Figure 14(b)]. The exact nature of the emission mechanism in semiconductor nanocrystallites is very complex and a clear picture has not yet emerged. Nevertheless, the photoluminescence arising from CdS nanoparticles is in general attributed to the surface defect emission and it is likely that the silica shell may influence it somehow. Figure 15 shows a comparison between the non-normalized PL spectra of SBA-16 SiO_2@CdS composite (i.e. a CdS-filled cage-like silica matrix) and the released CdS crystals after template removal. Notice the huge difference in intensity between both curves, especially bearing in mind that the SBA-16 SiO_2 matrix alone does not emit within the same wavelength range. It is therefore evident that the amorphous silica coverage of the CdS crystals enhances the PL response. Most importantly, because the CdS nanocrystals are

embedded within the silica matrix, it effectively protects the CdS from undesirable photoinduced oxidation (Wei et al, 2008).

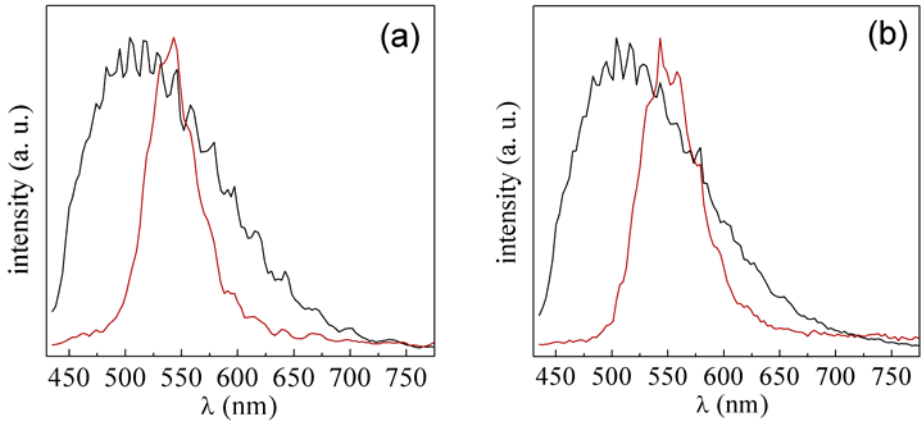

Fig. 14. Normalized PL spectra of (a) SBA-15 SiO_2@CdS composite (black curve) and *free* CdS nanocrystals (red curve), (b) KIT-6 SiO_2@CdS composite (black curve) and *free* CdS nanocrystals (red curve).

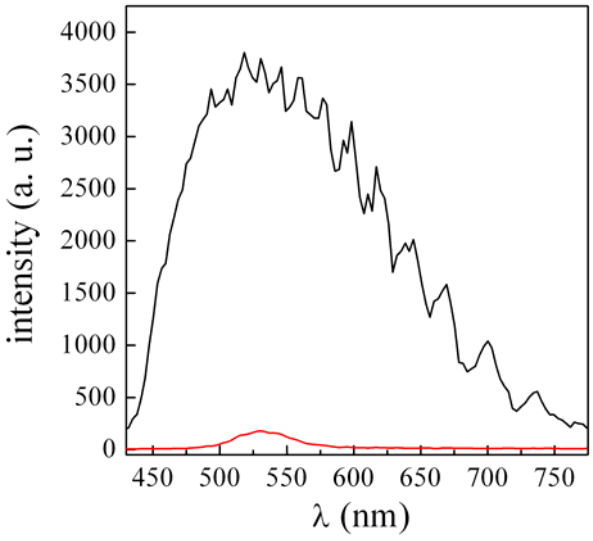

Fig. 15. Non-normalized PL spectra of SBA-16 SiO_2@CdS composite (black curve) and *free* CdS nanocrystals (red curve). Notice the huge difference in intensity between both curves, especially taking into account that the SB6-16 SiO_2 host alone does not emit.

5. Conclusion

The transition from microstructured to nanostructured engineering materials has been the subject of widespread research over the last years since nanocrystalline materials (i.e., nanostructured) can exhibit superior properties than conventional ones (i.e., microstructured). In particular, metal-ceramic (*cermet*) nanocomposites open a broad range of possibilities, aimed at utilizing in a synergetic way both the nanostructuring effects and the unique properties offered by metals and ceramics. Our results demonstrate that $SmCo_5$ nanoparticles trapped in NiO matrix exhibit tuneable and enhanced magnetic properties mostly depending on the $SmCo_5$ crystallite size. On the other hand, fine-tuning of the magnetic response is also feasible in oxide-oxide nanocast materials by combining ferrimagnetic ($NiCo_2O_4$) and antiferromagnetic (NiO and Co_3O_4) oxides. Moreover, these multiphase oxides present additional advantages such as moderately large surface areas due to their porous character and long-range order provided by the parent templates. Finally, semiconductor-silica composites show interesting optical properties thanks to the interface interaction between the semiconductor compound (CdS) and the silica shell. Examples presented here definitely demonstrate that oxide-based nanocomposites are suitable candidates for a wide range of innovative engineering applications.

6. Acknowledgements

We thank the Spanish MICINN (MAT2010-20616-C02) and the Catalan DGR (2009-SGR-1292) for partial financial support. E.P. is indebted to the Generalitat de Catalunya for the *Beatriu de Pinós* postdoctoral fellowship. M.D.B. acknowledges partial financial support from an ICREA-Academia Award.

7. References

Ajayan, P.M.; Schadler, L.S.; Braun P.V. (2003). *Nanocomposite science and technology*. Wiley-VCH, ISBN 3527303596, Weinheim.

Batlle, X. & Labarta, A. (2002). Finite-size effects in fine particles: magnetic and transport properties. *J. Phys. D: Appl. Phys.* 35, 6, R15-R42.

Beck, J. S.; Vartuli, J. C.; Roth, W. J.; Leonowicz, M. E.; Kresge, C. T.; Schmitt, K. D.; Chu, C. T. W.; Olson, D. H.; Sheppard, E. W. (1992). A new family of mesoporous molecular sieves prepared with liquid crystal templates. *J. Am. Chem. Soc.* 114, 27, 10834-10843.

Cabo, M.; Pellicer, E.; Rossinyol, E.; Estrader, M.; López-Ortega, A.; Nogués, J.; Castell, O.; Suriñach, S.; Baró, M. D. (2010). Synthesis of compositionally graded nanocast $NiO/NiCo_2O_4/Co_3O_4$ mesoporous composites with tunable magnetic properties. *J. Mater. Chem.* 20, 33, 7021-7028.

Hadjipanayis, G.C. (1999). Nanophase hard magnets. *J. Magn. Magn. Mater.* 200, 1-3, 373-391.

Kneller, E.F.; Hawig, R. (1991). The exchange-spring magnet – A new material principle for permanent magnets. *IEEE Trans. Magn.* 27, 4, 3588-3600.

Leslie-Pelecky D. L.; Schalek, R. L. (1999). Effect of disorder on the magnetic properties of $SmCo_5$. *Phys. Rev. B* 59, 1, 457-462.

Li, Y.; Zhu, Y.; Yang, X.; Li. C. (2008). Mesoporous Silica Spheres as Microreactors for Performing CdS Nanocrystal Synthesis. *Cryst. Growth Des.* 8, 12, 4494-4498.

Lu, A.-H.; Zhao, D.; Wan Y. (2010). *Nanocasting. A versatile strategy for creating nanostructured porous materials*. RSC Publishing, ISBN 978-0-85404-188-6, Cambridge.

Murty, B.S.; Ranganathan, S. (1998) Novel materials synthesis by mechanical alloying/milling. *Internat. Mater. Rev.* 43, 3, 101-141.

Nogués, J.; Schuller, I. K. (1999). Exchange bias. *J. Magn. Mang. Mater.* 192, 2, 203-232.

Sort, J.; Suriñach, S.; Muñoz, J.S.; Baró, M.D.; Nogués, J.; Chouteau, G.; Skumryev, V.; Hadjipanayis, G.C. (2002). Improving the energy product of hard magnetic materials. *Phys. Rev. B* 65, 17, 174420.

Schrefl, T.; Fidler, J.; Kronmüller. H. (1994) Remanence and coercivity in isotropic nanocrystalline permanent-magnets. *Phys. Rev. B* 49, 9, 6100-6110.

Strnat K.J.; Strnat, R.M.W. (1991). Rare earth cobalt permanent-magnets. *J. Magn. Magn. Mater.* 100, 1-3, 38-56.

Tiemann, M. (2008). Repeated templeating. *Chem. Mater.* 20, 3, 961-971.

Wang, S.; Choi, D.-G.; Yang, S.-M. (2002). Incorporation of CdS nanoparticles inside ordered mesoporous silica SBA-15 via ion-exchange. *Adv. Mater.* 14, 18, 1311-1314.

Wei, D.P.; Ma, Y.; Pan, H.Y.; Chen, Q. (2008). A versatile chemical vapor deposition method to synthesize one-dimensional silica-sheathed nanostructures. *J. Phys. Chem. C* 112, 23, 8594-8599.

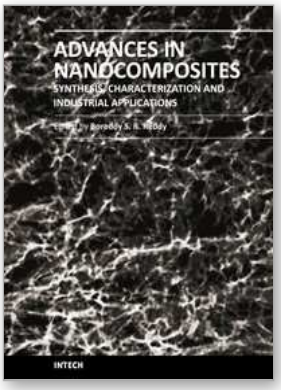

Advances in Nanocomposites - Synthesis, Characterization and Industrial Applications

Edited by Dr. Boreddy Reddy

ISBN 978-953-307-165-7
Hard cover, 966 pages
Publisher InTech
Published online 19, April, 2011
Published in print edition April, 2011

Advances in Nanocomposites - Synthesis, Characterization and Industrial Applications was conceived as a comprehensive reference volume on various aspects of functional nanocomposites for engineering technologies. The term functional nanocomposites signifies a wide area of polymer/material science and engineering, involving the design, synthesis and study of nanocomposites of increasing structural sophistication and complexity useful for a wide range of chemical, physicochemical and biological/biomedical processes. "Emerging technologies" are also broadly understood to include new technological developments, beginning at the forefront of conventional industrial practices and extending into anticipated and speculative industries of the future. The scope of the present book on nanocomposites and applications extends far beyond emerging technologies. This book presents 40 chapters organized in four parts systematically providing a wealth of new ideas in design, synthesis and study of sophisticated nanocomposite structures.

How to reference

In order to correctly reference this scholarly work, feel free to copy and paste the following:

Eva Pellicer, Emma Rossinyol, Moisés Cabo, Alberto López-Ortega, Marta Estrader, Santiago Suriñach, Maria Dolors Baró, Josep Nogués and Jordi Sort (2011). Oxide-Matrix Based Nanocomposite Materials for Advanced Magnetic and Optical Functionalities, Advances in Nanocomposites - Synthesis, Characterization and Industrial Applications, Dr. Boreddy Reddy (Ed.), ISBN: 978-953-307-165-7, InTech, Available from: http://www.intechopen.com/books/advances-in-nanocomposites-synthesis-characterization-and-industrial-applications/oxide-matrix-based-nanocomposite-materials-for-advanced-magnetic-and-optical-functionalities

INTECH
open science | open minds

InTech Europe
University Campus STeP Ri
Slavka Krautzeka 83/A
51000 Rijeka, Croatia
Phone: +385 (51) 770 447
Fax: +385 (51) 686 166
www.intechopen.com

InTech China
Unit 405, Office Block, Hotel Equatorial Shanghai
No.65, Yan An Road (West), Shanghai, 200040, China
中国上海市延安西路65号上海国际贵都大饭店办公楼405单元
Phone: +86-21-62489820
Fax: +86-21-62489821